Measurements of a Hamiltonian System and Their Description by a Diffusive Model

T. Chen,[1] A. Gerasimov,[2] B. Cole,[3] D. Finley,[2] G. Goderre,[2] M. Harrison,[2] R. Johnson,[2] I. Kourbanis,[2] C. Manz,[4] N. Merminga,[4] L. Michelotti,[2] S. Peggs,[2] F. Pilat,[3] S. Pruss,[2] C. Saltmarsh,[3] S. Saritepe,[2] T. Satogata,[2] R. Talman,[1] C. G. Trahern,[3] and G. Tsironis[5]

[1]*Newman Laboratory of Nuclear Studies, Cornell University, Ithaca, New York 14853*
[2]*Fermi National Accelerator Laboratory, Batavia, Illinois 60510*
[3]*Superconducting Super Collider Laboratory, Dallas, Texas 75237*
[4]*Stanford Linear Accelerator Center, Stanford, California 94305*
[5]*Physics Department, University of North Texas, Denton, Texas 76203*

(Received 15 August 1991; revised manuscript received 8 November 1991)

The dynamics of transverse particle oscillations in the Fermilab Tevatron, artificially made nonlinear, is studied by observing beam profiles over periods up to an hour. A "diffusive" model with amplitude-dependent diffusion coefficient gives a quantitatively accurate description of beam evolution. The evolution is influenced strongly by nonlinear resonance.

PACS numbers: 41.80.Gg, 03.20.+i, 05.45.+b, 29.20.Dh

This Letter describes a beam dynamics experiment, performed in the Fermilab Tevatron, that studied the effect of nonlinearity on transverse particle distributions. As well as being the study of an almost ideally Hamiltonian system, this investigation was motivated by planning for future accelerators, for which nonlinearity in the transverse motion will be of special importance. These effects are studied by adding artificial nonlinearity to the most similar existing accelerator, the Tevatron. For this experiment the Tevatron can be regarded as a linear system on which known nonlinearity in the form of sixteen sextupole magnets has been artificially superimposed. (In an earlier experiment using the same apparatus [1] phase-space features were measured quantitatively in a nonlinear configuration similar to the present one.) We concentrate here on "stochastic" effects, due to the particle dynamics, that cause "diffusive" evolution of the beam distribution even in the absence of external sources of "noise" or random scattering from residual gas molecules.

At the start of each observation period a needle-shaped single bunch of some 10^{10} circulating stored protons was kicked horizontally. This yielded displacement x_k (typically 3 mm) as observed at a downstream observation point. The resulting transverse beam profile was determined by measuring the instantaneous radioactivity as a fine wire was caused to fly through the beam repeatedly every minute or so. During a run of (typical) duration 30 min, each proton circulates some 10^8 times and executes some 2×10^9 transverse "betatron" oscillations. The purpose of the kick is to generate a beam in which all the particles are in a region of measurably large diffusion.

Individual protons oscillate at approximately constant amplitude with damping time equal to many tens of hours. The assumptions of Hamiltonian mechanics are probably as valid for this system as for any laboratory-observable phenomenon. One consequence of this is the certain validity of Liouville's theorem, according to which *microscopic* particle densities in phase space are conserved. The phase space referred to here describes motion in one transverse dimension (horizontal), with position and momentum coordinates being (x,p). In this paper the momentum is scaled to have the same units as x (millimeters), so that unperturbed phase-space trajectories are circles of radius $r\equiv\sqrt{J}=(x^2+p^2)^{1/2}$. Because of Liouville's theorem, an initial beam distribution depending only on r (except for distortion due to nonlinearity) would remain invariant. In spite of this, it is consistent with Liouville's theorem for void regions to be mixed into populated regions yielding a "foam" of reduced macroscopic density. That is the behavior studied in this experiment.

Two configurations, labeled A and B, were investigated. For them, individual sextupoles had the same strengths but the distributions of their polarities were selected to lead to strikingly different phase-space structure. For two "tune" settings at each of A and B the predicted phase-space trajectories are shown in Fig. 1. These are "Poincaré plots" taken at a fixed location ("surface of section") in the lattice, with a point plotted at the point (x,p) on each successive turn. (The tune is the fraction of 360° that successive points advance on each turn in such a plot.) The plots in Fig. 1 were generated by a symplectic numerical tracking program TEAPOT [2] using the known linear lattice and sextupole configuration in the Tevatron. As well as trajectory distortion, there is the possibility of "frequency entrainment" onto resonance islands (cases $A_>$ and $B_>$), and, at very large amplitude, particle loss due to the vacuum chamber wall or another material object. To make the physical aperture definite, a scraper was placed at $x_\infty=8$ mm. This value was chosen small enough to be certain to catch essentially all "doomed" particles, but large enough to make the observations insensitive to the actual value of x_∞. Both of these properties were verified experimentally. Though the precise location of this aperture is not critical, the loss of particles it causes is crucial to the evolution and survival of the beam.

In order to study the influence of resonance (though not the dominant strong third integer resonance) all measurements were performed in the vicinity of the "$\frac{2}{5}$ resonance" (fractional horizontal tune ν_x close to 0.4). This

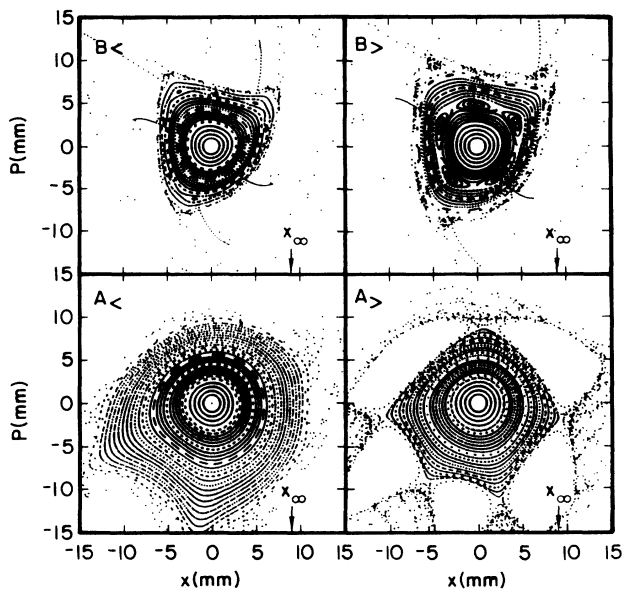

FIG. 1. Predicted Poincaré plots for the four nonlinear configurations studied. Identical starting coordinates were chosen for all plots. A and B indicate different sextupole distributions; $<$ and $>$ refer to just below and just above the dominant resonance. Note the five-island resonance chains in the $>$ cases. Other parameters are listed in Table I.

means that the motion approximately repeats every fifth turn. Configurations were intentionally chosen in pairs, such as $A_>$ and $A_<$, just above and just below resonance, respectively, with everything else held constant. For both sextupole distributions under study the tune decreases with increasing amplitude. This causes entrainment to occur, with the fractional tune locking onto exactly $\frac{2}{5}$, only in the $>$ cases. This is confirmed by Fig. 1. With the fractional tune so close to 0.4, resonances at other rational tune values are of minor importance.

The particle distribution in phase space is approximately described by a symmetric probability distribution depending only on r, not separately on x and p. For a brief interval after the beam is first kicked this is not true, but within less than 10^3 turns (negligibly short on the time scale of our observations), "filamentation" due to shear tangential motion leads to a distribution that uniformly fills a ring of radius x_k in phase space. We call a beam formed in this way a "hollow beam." The same rapid shear motion in phase space continues to preserve azimuthal symmetry even if the stochastic forces are asymmetric. It was shown by Landau [3] that the influence of stochastic forces on a distribution of Hamiltonian oscillators can be described by a one-dimensional diffusion equation

$$\frac{\partial \rho_j(J;t)}{\partial t} = \frac{\partial}{\partial J}\left[D_j(J)\frac{\partial \rho_j(J;t)}{\partial J}\right], \tag{1}$$

similar to, but not identical to, the radial heat equation in a cylindrically symmetric situation. (The difference is inconsequential. A complete reanalysis based on the heat equation was just as satisfactory as the fit we describe.) Here $D_j(J)$ is an amplitude-dependent diffusion coefficient to be determined by data fitting. The distribution function $\rho_j(J;t)$ is normalized to the intensity $N(t)$—the total number of particles surviving at time t, which we measure. Before the beam is kicked it has a Gaussian profile with a rms width σ_0 that was measured at the start of each run. The condition for the beam to be truly hollow is $\sigma_0 \ll x_k$. In actual cases $\sigma_0 = 1.1 \pm 0.1$ mm and $x_k > 2.4$ mm. Our apparatus measures the projection of this distribution onto the x axis. This profile is compared to a theoretical profile obtained by solving Eq. (1) numerically and projecting onto the x axis.

The evolution of beam profiles in electron storage rings in the presence of stochasticity caused by quantum fluctuations as well as damping due to radiation would undoubtedly be correctly described by a similar partial differential equation, though the standard treatment [4] is rather different.

Our model of the diffusive evolution is based on a four-parameter expression for the diffusion coefficient:

$$D_j(J) = \begin{cases} D_f, & \text{if } r < r_0, \\ D_f + d_0(J - J_0)^K, & \text{if } r_0 < r. \end{cases} \tag{2}$$

The most important parameter is $r_0 = J_0^{1/2}$, which can be regarded as a phase-space radius inside which there is no dynamics-induced diffusion (a kind of experimentally determined radius of the largest Kolmogorov-Arnold-Moser surface). Since the particle density is tailored initially to be large only in a reasonably slender radial ring, the diffusion coefficient is best determined near there. At larger amplitudes, other than being required by the data to be large, the diffusion coefficient is poorly determined. In the particular parametrization chosen, the rate at which diffusion increases as r exceeds r_0 is controlled by the coefficient d_0 and the exponent K. The parameter D_f represents uniform diffusion, such as could be caused by external sources of noise, but it was allowed to vary from configuration to configuration. Model profiles are obtained by solving Eq. (1) with the diffusion coefficient given by Eq. (2), with boundary conditions that forbid a sink at $J = 0$ and force a zero at $r = x_\infty$. Resulting profiles are shown in Fig. 2. The smooth curves are profiles predicted at the times indicated. The jagged curve is one raw profile measured by the flying wire system. It is typical of the hundreds of profiles measured. The jagged nature of these profiles was somewhat smoothed before comparison with the model; this accounts for the jagged curve being somewhat narrower than the smooth curve predicted at the same time.

In performing fits to determine the parameters in D_j, only two measures of the observed distributions were used—the total area, proportional to $N(t)$, and the full width at half maximum. For each of the configurations studied, data sets like those in Fig. 3 were taken. Pairs of small-kick and large-kick runs were taken, differing only

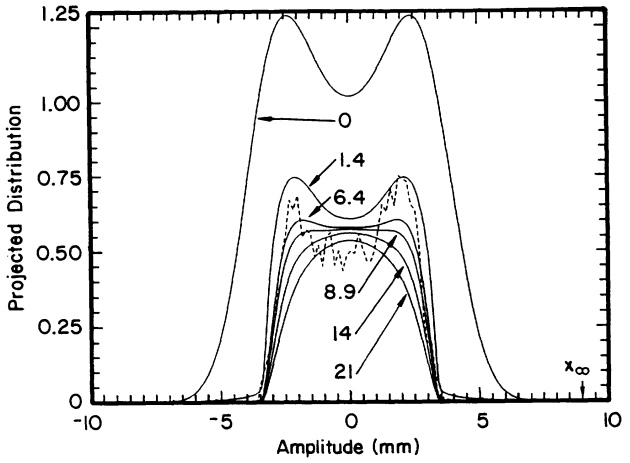

FIG. 2. Evolution of the beam profile as predicted by the diffusion model: smooth curves. Times (in minutes after hollow beam formation) are indicated. The jagged curve is the raw flying wire measurement of the profile at $t=6$ min.

in the value of x_k, which was adjusted by controlling the kicker voltage V_k [$x_k(\text{mm}) \simeq 0.47 V_k(\text{kV})$]. The values are indicated in Fig. 3. The idea was to bracket r_0 by preferentially populating a low-diffusion region in one run and a high-diffusion region in the other. A data-collection grid more narrowly spaced in V_k was neither permitted by time nor justified by the inherent size σ_0 of the prekicked beam. "Best-fit" parameters minimize the sum of the squares of deviations on these four plots. They are listed in Table I. The errors listed are calculated under the assumption that deviations from the best-fit curves are purely statistical, and that the deviations can be used to estimate error bars (assumed equal) for individual points. The parameters are reasonably uncorrelated statistically; with normalization making diagonal terms of the covariance matrix 1, no off-diagonal term exceeds 0.2 in magnitude. From the smallness of the errors, it can be seen that each given data set determines the fit parameters sharply, but without more careful specification of conditions the errors have limited significance. In particular, extrapolation of the diffusion coefficient into regions that were not populated experimentally is clearly invalid.

Defining "foreground" data to be that taken with sextupoles turned on, "background" data were taken using the bare Tevatron. Bare Tevatron data taken at a kick value of 9 keV showed negligible diffusion, and TEAPOT tracking in that region, using measured field deviations, showed the motion to be essentially linear. Paired data sets with kick voltages of 12 and 14 kV were taken and the results were analyzed using the diffusion coefficient parametrization of Eq. (2). The best-fit value of parameter r_0 in this case was determined to be 6.5 mm, though the fit was not very good. On these bases "background" diffusion was neglected, other than through its empirical representation by D_f.

A consistency check made toward the end of some runs was to reduce x_∞ suddenly. An example is Fig. 3, 27 min into the run. This tested how well the subsequent beam

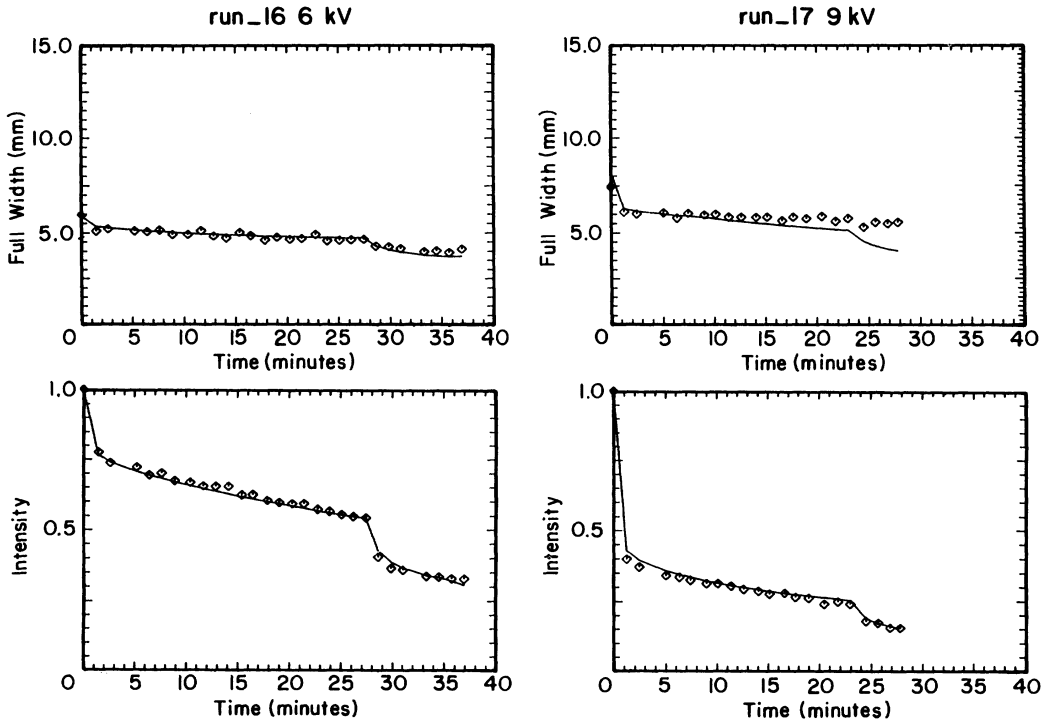

FIG. 3. Measured full widths and intensities (points) compared to model-derived values (smooth curve). Intensities are normalized to 1 at $t=0$. The step discontinuities at late times are the result of sudden reductions of x_∞ to 2.7 mm. The quality of the fit for all data points was comparable to this.

TABLE I. Diffusion coefficient parameters.

Parameter units	Kicks (kV)	ν_x	d_0	r_0 (mm)	K	D_f (mm^4/min)	r_0/Δ
$A<$	6,9	20.392	215 ± 2.4	488 ± 0.02	1.19 ± 0.01	4.7 ± 0.01	0.42
$A>$	6,9	20.408	118 ± 2.1	3.90 ± 0.02	1.68 ± 0.01	2.9 ± 0.02	0.44
$B<$	6,9	20.392	9.0 ± 0.33	3.40 ± 0.02	1.88 ± 0.01	0.87 ± 0.01	0.51
$B>$	6,9	20.408	160 ± 4.8	3.54 ± 0.04	1.30 ± 0.02	3.0 ± 0.03	0.51

evolution was described by the same diffusion coefficient and the model profile in existence at that time. These fits are unfortunately very sensitive to small uncertainties in the absolute scraper location. A 1.3-mm discrepancy between nominal and best-fit values was judged to be consistent with absolute position uncertainties in the setup. With this adjustment, the excellent fits to the 6-kV data of Fig. 3 result. However, without parameter readjustment, the 9-kV full-width fit is not very good. The source of this discrepancy is not understood. It is also not understood why the best-fit value of D_f varies from configuration to configuration.

For comparison with Fig. 1, the final column of Table I gives the ratio r_0/Δ; $\Delta=(x_{\max}-x_{\min})/2$, where $x_{\min}$ and $x_{\max}$ are the extremes of regular motion along the x axis.

The discussion has assumed that the motion is purely horizontal. In fact, individual particles are also undergoing appreciable vertical oscillation at a tune of $\nu_y=20.45$. Before being kicked the beam is approximately round and the kick does not alter the vertical motion. As a result, the beam is ribbon shaped after the kick with relatively small vertical motion. However, it cannot be assumed that horizontal diffusion is uninfluenced by this motion. Our diffusion coefficient has to be regarded as including this influence. The same comments can be made about longitudinal motion ($\nu_s=0.0016$). In addition, because the flying wire is located at a point HE11 having nonzero dispersion, the momentum oscillations accompanying this motion broaden the observed profiles slightly. To study this effect we performed a complete reanalysis of the data, approximately taking this into account; the alteration was judged to be too small to justify the extra complexity. In summary, our diffusion coefficient is intended to account phenomenologically for the evolution of horizontal profiles in the presence of small vertical and longitudinal motion.

Qualitative inferences about the nature of the diffusion process can be tentatively drawn. Contrary to intuition, and unlike multiple scattering, diffusion causes the beam to narrow with time. This behavior is caused by the sink at x_∞ which devours large-amplitude particles, reduces the beam intensity, and depletes the tail of the distribution. The feature of the data most naturally demanding a diffusive description is the enormous range of time scales involved. At small amplitudes the time scale is so long that diffusion can be neglected; the time scale at large amplitudes is negligibly short. The full range is smoothly encompassed by dependence (2). The hollow beam rapidly (in 10^6 turns) sheds its large-amplitude particles and the periphery of the distribution approaches what appears to be a universal shape. This is stable indefinitely except that weak diffusion occasionally brings particles to the "edge" from where they quickly "evaporate."

The calculations of Fig. 1 can be compared with the experimental data, parametrized according to Eq. (2), and listed in Table I. The near constancy of the ratio r_0/Δ shows that theory and observation are consistent. As a rule of thumb, based on this ratio, one can conjecture that diffusion causes particles outside roughly $(0.47\pm0.04)\Delta$ to be lost rapidly. (The "realistic aperture" is about half of the "optimistic aperture.") Relatively greater diffusion in case $A>$ than case $A<$ is made manifest by a small value of r_0. Relatively greater diffusion in case $B>$ than case $B<$ is made manifest by a large value of d_0. Both suggest that the diffusion rate is enhanced by proximity to resonance. Certainly it is routinely observed that beam loss in accelerator operations is aggravated by resonance.

We gratefully acknowledge the work of Keng Low, Matthew Kane, Michael Allen, Vern Paxson, Soam Acharya, and Kevin Cahill for their help in configuring the data-acquisition system, and the Fermilab operations staff. Also, for helpful discussions, we thank George Bourianoff.

[1] A. Chao *et al.*, Phys. Rev. Lett. **61**, 2752 (1988).
[2] L. Schachinger and R. Talman, Part. Accel. **22**, 35 (1987).
[3] L. D. Landau, ascribed to Zh. Eksp. Teor. Fiz. **7**, 203 (1937), by A. J. Lichtenberg and M. A. Lieberman, *Regular and Stochastic Motion* (Springer-Verlag, New York, 1983).
[4] M. Sands, SLAC Report No. SLAC-121, 1970 (unpublished).

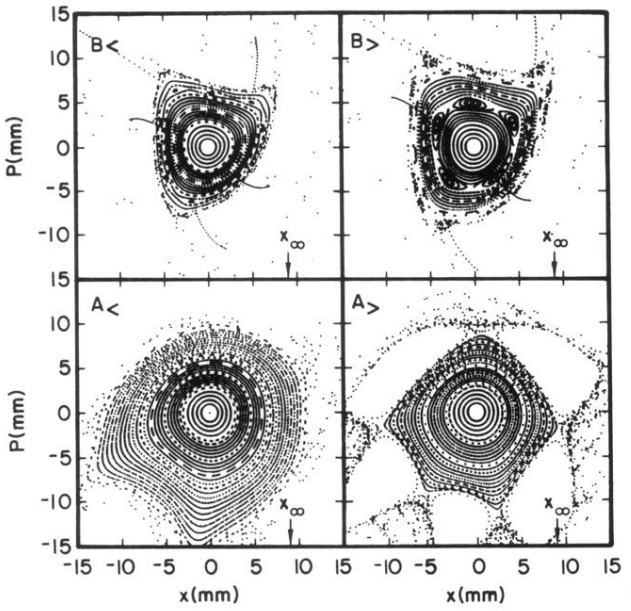

FIG. 1. Predicted Poincaré plots for the four nonlinear configurations studied. Identical starting coordinates were chosen for all plots. *A* and *B* indicate different sextupole distributions; < and > refer to just below and just above the dominant resonance. Note the five-island resonance chains in the > cases. Other parameters are listed in Table I.